Systematic deletions in the cellobiohydrolase (CBH) Cel7A from the fungus Trichoderma reesei reveal flexible loops critical for CBH activity

Schiano-de-Cola, Corinna; Røjel, Nanna; Jensen, Kenneth; Kari, Jeppe; Sørensen, Trine Holst; Borch, Kim; Westh, Peter

Published in:
Journal of Biological Chemistry

Link to article, DOI:
10.1074/jbc.RA118.006699

Publication date:
2019

Document Version
Publisher's PDF, also known as Version of record

Systematic deletions in the cellobiohydrolase (CBH) Cel7A from the fungus *Trichoderma reesei* reveal flexible loops critical for CBH activity

Received for publication, November 13, 2018, and in revised form, December 8, 2018 Published, Papers in Press, December 11, 2018, DOI 10.1074/jbc.RA118.006699

Corinna Schiano-di-Cola[‡1,2], Nanna Røjel[‡1,2], Kenneth Jensen[§], Jeppe Kari[‡], Trine Holst Sørensen[‡], Kim Borch[§], and Peter Westh[¶3]

From [‡]the Department of Science and Environment, Roskilde University, Universitetsvej 1, Building 28, DK-4000 Roskilde, Denmark, [§]Novozymes A/S, Krogshøjvej 36, DK-2880 Bagsværd, Denmark, and [¶]the Department of Biotechnology and Biomedicine, Technical University of Denmark, Building 224, DK-2800 Kgs. Lyngby, Denmark

Edited by Gerald W. Hart

Glycoside hydrolase family 7 (GH7) cellulases are some of the most efficient degraders of cellulose, making them particularly relevant for industries seeking to produce renewable fuels from lignocellulosic biomass. The secretome of the cellulolytic model fungus *Trichoderma reesei* contains two GH7s, termed TrCel7A and TrCel7B. Despite having high structural and sequence similarities, the two enzymes are functionally quite different. TrCel7A is an exolytic, processive cellobiohydrolase (CBH), with high activity on crystalline cellulose, whereas TrCel7B is an endoglucanase (EG) with a preference for more amorphous cellulose. At the structural level, these functional differences are usually ascribed to the flexible loops that cover the substrate-binding areas. TrCel7A has an extensive tunnel created by eight peripheral loops, and the absence of four of these loops in TrCel7B makes its catalytic domain a more open cleft. To investigate the structure–function relationships of these loops, here we produced and kinetically characterized several variants in which four loops unique to TrCel7A were individually deleted to resemble the arrangement in the TrCel7B structure. Analysis of a range of kinetic parameters consistently indicated that the B2 loop, covering the substrate-binding subsites −3 and −4 in TrCel7A, was a key determinant for the difference in CBH- or EG-like behavior between TrCel7A and TrCel7B. Conversely, the B3 and B4 loops, located closer to the catalytic site in TrCel7A, were less important for these activities. We surmise that these results could be useful both in further mechanistic investigations and for guiding engineering efforts of this industrially important enzyme family.

The cellulases Cel7A and Cel7B are abundant both in the secretome of the cellulolytic fungus *Trichoderma reesei* and enzyme mixtures for the industrial deconstruction of lignocellulosic biomass (1–4). These two enzymes are homologs and share the same overall fold with almost 50% amino acid sequence identity (1). Nevertheless, they attack their insoluble substrate in quite different manners. Cel7A from *T. reesei* (TrCel7A) is a typical processive cellobiohydrolase (CBH)[4] that targets the reducing end of a cellulose strand and subsequently makes consecutive cuts that release cellobiose as the enzyme moves along the strand (5–9). Conversely, TrCel7B is categorized as an endoglucanase (EG) that typically targets the strand internally and shows little or no processivity (10, 11). TrCel7A and TrCel7B are also quite different with respect to their ability to hydrolyze different types of cellulose. Hence, TrCel7A is among the most efficient enzymes for the breakdown of crystalline cellulose. TrCel7B shows very limited activity against crystalline substrate, but effectively hydrolyzes amorphous parts of the cellulose (10, 12, 13). Moreover, in terms of kinetics, TrCel7A and TrCel7B display several opposite characteristics: TrCel7B has a much higher turnover frequency than TrCel7A (14), decreased product inhibition (15, 16), and lower adsorption on cellulose compared with TrCel7A (17). These differences play a key role in the cellulolytic capacity of the fungal secretome as they promote conversion of heterogeneous substrates with different cellulose structure and give rise to a distinctive synergy between the two enzymes (12, 18–20). In light of this, it is interesting to consider why structural homologs harbor these functional differences. The main structural differences between TrCel7A and TrCel7B are found in the flexible loops that cover the active site (21–23). TrCel7A has a total of eight such loops that form the tunnel. There are four loops on each side termed A1–A4 and B1–B4, respectively (24). In TrCel7B, four of these loops (A4, B2, B3, and B4) are truncated to an extent where they are essentially absent (23). This results in a more open and accessible substrate-binding cleft in TrCel7B, as illustrated in Fig. 1*A*. Several earlier studies have suggested that the functional differences between CBHs and EGs can be attributed to loop configuration (25). As an example, Meinke *et al.* (26) explored the importance of the loops for

This work was supported by Innovation Fund Denmark Grant 5150-00020B (to P. W.) and Novo Nordisk Foundation Grant NNF15OC0016606. K. J. and K. B. are employed by Novozymes, a major enzyme-producing company.
This article contains Figs. S1–S3.

[1] Both authors contributed equally to this work.

[2] Present address: Dept. of Biotechnology and Biomedicine, Technical University of Denmark, Bldg. 224, DK-2800 Kgs. Lyngby, Denmark.
[3] To whom correspondence should be addressed. Tel.: 45-4525-2641; E-mail: petwe@dtu.dk.

[4] The abbreviations used are: CBH, cellobiohydrolase; AZCL-HE-cellulose, azurine-cross-linked hydroxyethylcellulose; EG, endoglucanase; DSC, differential scanning calorimetry; pNPL, *para*-nitrophenyl β-D-lactopyranoside; RAC, regenerated amorphous cellulose; BMCC, bacterial microcrystalline cellulose; PDB, Protein Data Bank; BisTris, 2-[bis(2-hydroxyethyl)amino]-2-(hydroxymethyl)propane-1,3-diol; PAHBAH, 4-hydroxybenzoic acid hydrazide.

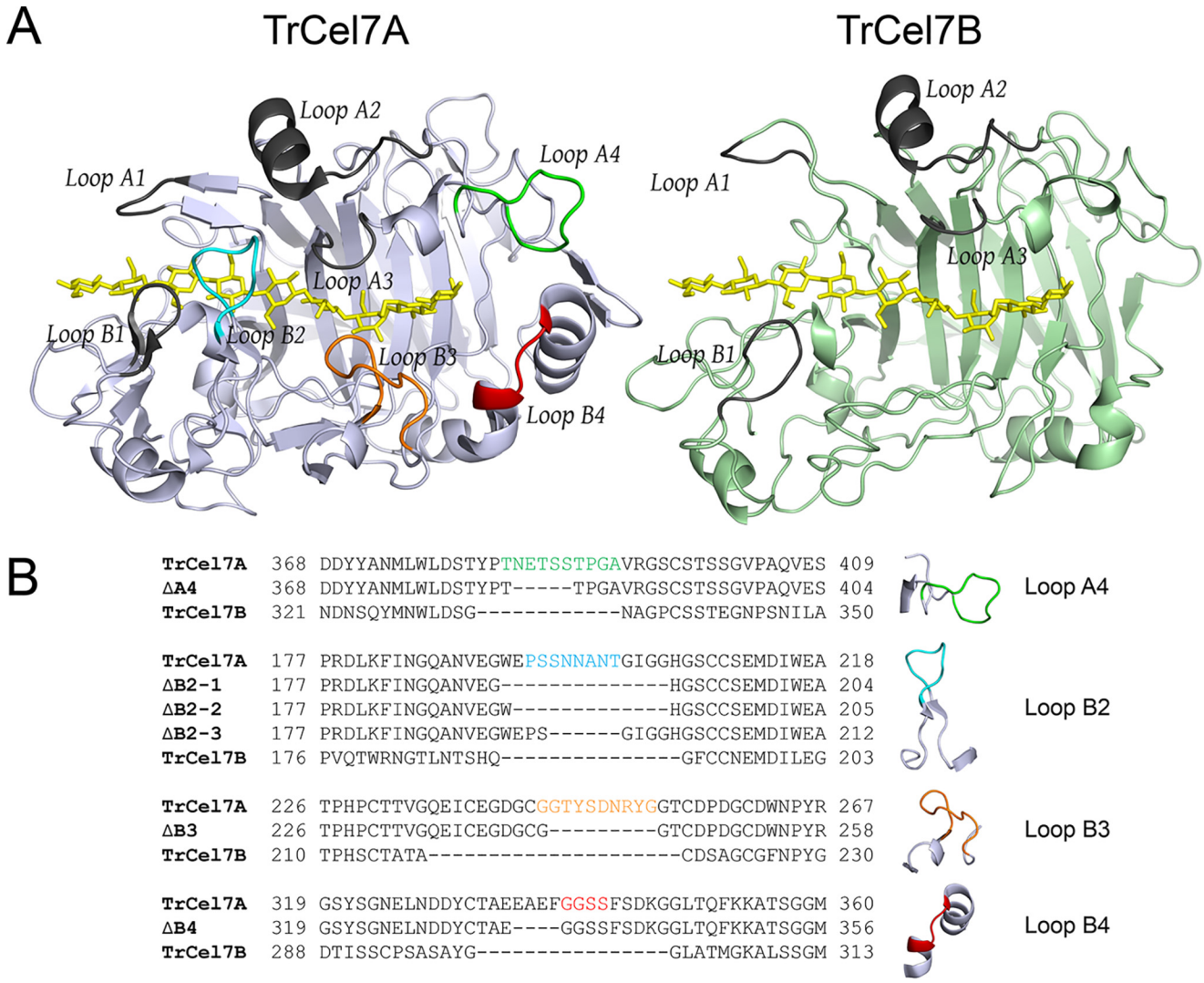

Figure 1. Structure of TrCel7A and TrCel7B with highlighted loops and sequence alignments. *A*, *cartoon representation* of TrCel7A (PDB entry 4C4C) and TrCel7B (PDB entry 1EG1) with cellononaose in *yellow sticks*. The substrate structure was taken from 4C4C and superimposed onto TrCel7B. The loops that cover the substrate-binding tunnel or cleft are *highlighted* in *different colors*. Loops that are common between the two enzymes are *highlighted* in *black* (A1–A3 and B1 loops). Loops unique to TrCel7A are *highlighted* in *different colors*: A4 loop (*green*), B2 loop (*cyan*), B3 loop (*orange*), and B4 loop (*red*). *B*, amino acid sequence alignments of the different loop regions of TrCel7A, loop deletion (Δ) variants of TrCel7A, and TrCel7B. The deletion mutants lack the residues Asn^{384}–Ser^{388} for ΔA4, Trp^{192}–Gly^{205} for ΔB2-1, Glu^{193}–Gly^{205} for ΔB2-2, Ser^{196}–Thr^{201} for ΔB2-3, Gly^{245}–Gly^{253} for ΔB3, and Glu^{335}–Phe^{338} for ΔB4. The *dashed lines* indicate the regions missing in the different sequences compared with TrCel7A. The loop nomenclature and the *color coding* are the same as in *A*. The loops of interest are illustrated on the *right*.

distinguishing between exo- and endolytic activity in a GH6 cellulase. In that case, one of the two main loops that covered the active site was deleted, which increased the endolytic activity. Furthermore, Von Ossowski *et al.* (27) showed that a deletion in the B3 loop (*c.f.* Fig. 1*A*) in TrCel7A caused a decrease in activity on crystalline cellulose but increased activity on amorphous substrate. This latter variant also showed decreased processivity and product inhibition and hence a more EG-like behavior. In addition to these experimental studies, several computational works (11, 24, 28–30) have expanded our understanding of the loop properties in TrCel7A.

In the current work, we have investigated the functional role of TrCel7A loops. We focused on the four loops that are absent in TrCel7B and their role in the regulation of CBH- and EG-type activity. Specifically, we conducted comprehensive kinetic studies of the two WTs, TrCel7A and TrCel7B, and a group of TrCel7A variants in which these loops were trimmed individually.

Results and discussion

Design and expression

Six variants were designed based on pairwise sequence and structural alignments of TrCel7A and TrCel7B. The variants were constructed by systematically deleting individual loops of TrCel7A to mimic the corresponding regions of TrCel7B, as specified in Fig. 1. Three variants with different degree of truncation of the B2 loop were made. One, henceforth termed ΔB2-1, had a 14-amino acid deletion (ΔTrp^{192}–Gly^{205}), whereas the two others had deletions of 13 (ΔGlu^{193}–Gly^{205}) and 6 amino acids (ΔSer^{196}–Thr^{201}), termed ΔB2-2 and ΔB2-3, respectively. Two other variants, termed ΔA4 and ΔB3, had deletions in the A4 loop

Table 1

Results from basic characterization of TrCel7A, TrCel7B, and the six loop truncation variants

The thermal stability, T_m, was determined as the transition midpoint in DSC (conditions: 0.5 mg/ml enzyme, 20–95 °C, scan rate 3.3 °C), and the three kinetic parameters k_{cat}, K_m, and the cellobiose inhibition constant K_i were derived from kinetic experiments using pNPL as substrate (conditions: 0.16–5 mM pNPL, 0.5 μM enzyme, 25 °C, 30 min). K_i was estimated from similar experiments in the presence of 100 and 200 μM cellobiose or from 2 and 4 mM cellobiose for TrCel7B. n.d., not determined.

Enzyme	T_m	k_{cat}	K_m	K_i (cellobiose)	Type of inhibition
	°C	s^{-1}	mM	μM	
TrCel7A	66.9	0.089 ± 0.001	0.78 ± 0.03	21 ± 0.8	Competitive
ΔA4	57.7	n.d.	n.d.	n.d.	n.d.
ΔB2-1	61.9	0.055 ± 0.001	0.89 ± 0.07	32 ± 2.3	Competitive
ΔB2-2	62.9	0.108 ± 0.002	0.80 ± 0.04	24 ± 1.0	Competitive
ΔB2-3	65.3	0.079 ± 0.001	0.76 ± 0.03	22 ± 0.6	Competitive
ΔB3	65.9	0.283 ± 0.007	3.40 ± 0.14	133 ± 8	Mixed[a]
ΔB4	59.0	0.080 ± 0.001	0.70 ± 0.03	46 ± 2	Competitive
TrCel7B	65.8	4.8 ± 0.7	11.12 ± 2.14	5300 ± 500	Competitive

[a] For mixed inhibition of ΔB3, α, the ratio of the two inhibition constants in the mixed mechanism, was 5.0 ± 2.0.

(ΔAsn^{384}–Ser^{388}) or the B3 loop (ΔGly^{245}–Gly^{253}), respectively. The last variant, named ΔB4, had a deletion of 4 amino acids (ΔGlu^{335}–Phe^{338}). Although this area is not considered part of the B4 loop in the assignment proposed by Momeni *et al.* (24), sequence alignment indicates that deleting this region could create a variant more similar to TrCel7B, where an entire α helix is absent (α2 in Fig. S1). All variants and their names are listed in Fig. 1, and a more thorough account of the alignment may be found in Fig. S1.

Basic characterization

We first made a general characterization to assess whether the loop variants were pure, stable, and active. In this work, we used a soluble substrate analog. A more detailed characterization of the activity on real cellulosic substrate will be discussed below.

The purified enzymes (WTs and variants) showed a single band in SDS-PAGE, and their monomeric status was confirmed by size-exclusion chromatography (see Figs. S2 and S3). Next, we measured thermal stability by differential scanning calorimetry (DSC) and kinetic parameters for the hydrolysis of the substrate *para*-nitrophenyl β-D-lactopyranoside (pNPL). Results of this work are listed in Table 1. Stability and kinetic constants for WT TrCel7A were similar to previously reported values (31, 32). DSC measurements showed that all variants had a small to moderate lowering of the transition temperature, T_m. The most unstable variant was ΔA4, with a loss of T_m of about 10 °C. Functionally, this variant was also severely impaired, and this most likely reflects that the tested truncation of the A4 loop led to major structural changes in the variant. By contrast, the three ΔB2 variants showed moderate decrease in T_m and only small changes in kinetic parameters on pNPL (k_{cat}, K_m, and cellobiose inhibition constant K_i; Table 1) compared with WT TrCel7A. The ΔB3 variant had essentially unchanged stability but was different from the WT with respect to kinetic parameters on pNPL. Specifically, k_{cat}, K_m, and K_i (cellobiose) were all increased by some 3–5-fold compared with WT TrCel7A. This kinetic behavior for a variant with truncated B3 loop has been reported before (27), and in this latter work, it was shown by crystallography that the deletion did not lead to structural disturbances. In light of this kinetic resemblance and small changes in T_m, it appears that the ΔB3 variant accommodated the mutation without major structural changes. Finally, the ΔB4 variant showed kinetic parameters on pNPL and an inhibition constant very similar to that of the WT. This also supported the view of a mainly conserved overall fold of the variant, albeit with lowered thermostability (ΔT_m = 7.9 °C).

In conclusion, the basic characterization suggested that five variants with truncations in either the B2, B3, or B4 loop could accommodate the deletions without major changes in their properties, and we consequently used these variants in the comparative analyses on real insoluble cellulose. The ΔA4 variant, on the other hand, appeared severely changed and hence inapt for further comparisons of loop effects.

Binding and enzyme kinetics on Avicel

Microcrystalline cellulose Avicel, which has comparable fractions of crystalline and amorphous cellulose (10), was used as substrate for the primary characterization of all enzymes with respect to steady-state kinetics and adsorption. We first used conventional Michaelis–Menten (MM) kinetics, where the initial rate, v_0, was estimated in experiments with low enzyme concentration and variable substrate loads. The results (Fig. 2*A*) were analyzed with respect to the MM equation,

$$v_0 = \frac{^{conv}V_{max} S_0}{^{conv}K_m + S_0} \quad \text{(Eq. 1)}$$

using nonlinear regression, and the resulting parameters, $^{conv}V_{max}/E_0$ and $^{conv}K_m$, are listed in Table 2. The superscript "conv" specifies that these parameters were measured by the conventional approach (*i.e.* with excess of substrate). Kinetic parameters for TrCel7A on Avicel were in agreement with an earlier study (31). Results for the two WTs in Table 2 showed that the maximal specific rate and the Michaelis constant were an order of magnitude higher for TrCel7B ($^{conv}V_{max}/E_0 \sim 2\ s^{-1}$ and $^{conv}K_m \sim 44$ g/liter) compared with TrCel7A (~0.2 s^{-1} and ~4 g/liter). Interestingly, the specificity constant,

$$^{conv}\eta = \frac{^{conv}V_{max}}{^{conv}K_m E_0} \quad \text{(Eq. 2)}$$

was essentially the same for all enzymes (WTs and variants) (Table 2). This implies that the catalytic efficacy was approximately the same and further supports the view that the variants accommodated the loop truncations without major structural disturbances. Returning to the kinetic parameters of the two WTs, the results were in line with the interpretation

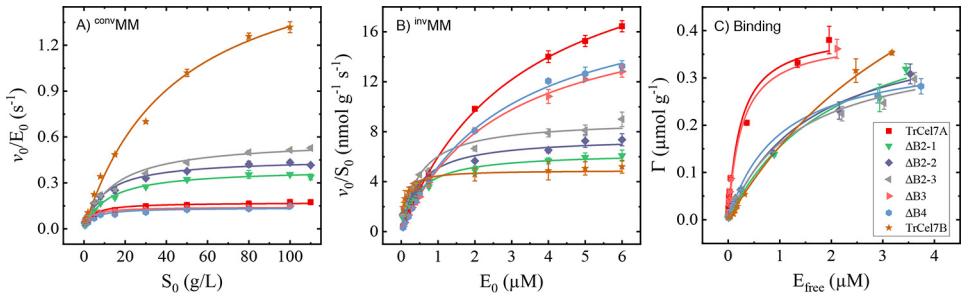

Figure 2. Conventional Michaelis–Menten, inverse Michaelis–Menten plots, and binding isotherms for TrCel7A (*red*), TrCel7B (*brown*), and deletion variants ΔB2-1 (*green*), ΔB2-2 (*purple*), ΔB2-3 (*gray*), ΔB3 (*pink*), and ΔB4 (*light blue*). Steady-state initial rates of hydrolysis are plotted against the Avicel substrate load (S_0) at a constant enzyme concentration (*A*) (conditions: 0.5–110 g/liter Avicel, 50 nM enzyme, pH 5, 60 min, 25 °C) or against the enzyme concentration (E_0) at a constant substrate load (*B*) (conditions: 8 g/liter Avicel, 0.05–6 μM enzyme, pH 5, 60 min, 25 °C). Binding isotherms on Avicel (*C*) are performed in the same conditions as *B*. *Symbols*, experimental data with S.D. (*error bars*); *lines*, best fit for the different equations.

Table 2

Steady-state kinetic and binding parameters and attack site density of TrCel7A, TrCel7B, and the variants ΔB2-1, ΔB2-2, ΔB2-3, ΔB3, and ΔB4 using Avicel as substrate

Parameters are derived from experiments shown in Fig 2.

Enzyme	convMM			invMM		Kinetic substrate accessibility (Γ_{attack})	Adsorption isotherms	
	$^{conv}V_{max}/E_0$	$^{conv}K_m$	$^{conv}\eta$	$^{inv}V_{max}/S_0$	$^{inv}K_m$		Γ_{max}	K_d
	$s^{-1} \times 10^{-3}$	g/liter	(liter g^{-1} s^{-1}) $\times 10^{-3}$	(μmol g^{-1} s^{-1}) $\times 10^{-3}$	μM	μmol/g	μmol/g	μM
TrCel7A	172 ± 6	4 ± 0.7	43 ± 8	25 ± 0.4	3.2 ± 0.10	0.147	0.40 ± 0.03	0.24 ± 0.06
ΔB2-1	391 ± 8	12 ± 1.0	33 ± 3	6 ± 0.2	0.5 ± 0.06	0.016	0.48 ± 0.04	2.13 ± 0.41
ΔB2-2	458 ± 12	10 ± 1.0	46 ± 5	8 ± 0.3	0.5 ± 0.07	0.016	0.43 ± 0.04	1.56 ± 0.33
ΔB2-3	583 ± 19	15 ± 1.8	39 ± 5	9 ± 0.3	0.5 ± 0.06	0.015	0.38 ± 0.03	1.32 ± 0.29
ΔB3	142 ± 5	3 ± 0.5	47 ± 8	19 ± 0.3	2.7 ± 0.11	0.131	0.39 ± 0.03	0.26 ± 0.07
ΔB4	138 ± 7	4 ± 1.0	35 ± 9	20 ± 0.5	2.8 ± 0.15	0.144	0.36 ± 0.01	0.99 ± 0.09
TrCel7B	1908 ± 97	44 ± 5.1	43 ± 5	5 ± 0.1	0.1 ± 0.02	0.003	0.87 ± 0.10	4.60 ± 0.78

that $^{conv}V_{max}$ is limited by slow dissociation from the substrate (5, 33) and hence that the comparably low maximal rate for TrCel7A is linked to its strong binding to the substrate (34). This higher affinity of TrCel7A is reflected in a low $^{conv}K_m$ in Table 2. TrCel7B, on the other hand, binds the substrate less tightly (10-fold higher $^{conv}K_m$), and this allows faster dissociation and hence higher $^{conv}V_{max}$. In the current context, it is interesting to relate this relationship of rate and affinity to loop morphology. Thus, stronger substrate interaction of TrCel7A may rely, at least in part, on the extensive loop coverage of the substrate-binding tunnel, which enables numerous enzyme–ligand contacts that are not found in TrCel7B (29). The additional interactions in TrCel7A manifest themselves in the kinetic data, as argued above, and in the following, we will use this relationship to assess functional roles of the loops from the kinetic properties of the variants. First, we note that deletions in the B3 or B4 loops only brought about marginal changes in $^{conv}V_{max}/E_0$ and $^{conv}K_m$. This means that these variants maintained the high substrate affinity and low turnover number that is characteristic for TrCel7A and hence that the B3 and B4 loops were not critical for ligand interaction. By contrast, any of the three tested deletions in the B2 loop significantly increased both $^{conv}V_{max}/E_0$ and $^{conv}K_m$ (Table 2), suggesting that the B2 loop plays a key role in substrate binding. These observations suggest that loss of the B2 loop made TrCel7A much more "EG-like" than loss of either the B3 or B4 loop. In the following, we will analyze other functional data along the same lines, to further elucidate how the investigated loops control the balance between typical EG and CBH behavior of TrCel7 enzymes.

Whereas the conventional MM equation can be applicable to the current system (35, 36), it has been suggested that a so-called inverse MM approach offers more robust steady-state analysis for cellulases (37, 38). In this inverse approach, the roles of enzyme and substrate are swapped, so that enzyme is in excess in the experiments and saturation represents a situation where all sites on the solid surface are occupied (with additional free enzyme in the aqueous phase). To perform this type of analysis, we measured the initial rate at low substrate load and a range of enzyme concentrations. Results in Fig. 2*B* were analyzed with respect to the inverse MM equation (39),

$$v_0 = \frac{^{inv}V_{max}E_0}{^{inv}K_m + E_0} \quad \text{(Eq. 3)}$$

using nonlinear regression, and the resulting parameters $^{inv}V_{max}/S_0$ and $^{inv}K_m$ are listed in Table 2. Interestingly, these inverse parameters confirm the overall picture from the conventional MM, in the sense that the parameters for all ΔB2 variants shifted strongly toward the EG, whereas ΔB3 and ΔB4 only shifted slightly. This again underscores the importance of the B2 loop for the function of TrCel7A. To illustrate the molecular meaning of the inverse parameters, we note that the inverse maximal rate, $^{inv}V_{max}$, will scale with the number of attack sites on the surface of the cellulose particle. The more sites on which the enzyme can bind and form a productive complex, the higher the $^{inv}V_{max}$. One consequence of this is that the number of attack sites per gram of cellulose, Γ_{attack}, can be roughly estimated as the ratio of maximal specific rates from the inverse and conventional MM analysis (37).

$$\Gamma_{attack} = \frac{^{inv}V_{max}/S_0}{^{conv}V_{max}/E_0} \quad \text{(Eq. 4)}$$

Results for Γ_{attack} in Table 2 reveal distinctive differences between TrCel7A and TrCel7B. The number of attack sites recognized per gram of Avicel is some 50-fold higher for TrCel7A compared with TrCel7B. This ability of TrCel7A to attack a broad range of structures on the heterogeneous surface has been reported before (40), and the distinctively reduced value for the homologous TrCel7B points toward loop morphology as a key determinant of this ability. Although molecular interpretations of this difference await further experimental work, we conclude that TrCel7A is promiscuous with respect to the conformation of the cellulose strand it attacks, whereas TrCel7B is a selective enzyme, which is only capable of forming catalytically competent complexes with a small subset of sites on Avicel. When considering Γ_{attack} for the variants, it appeared that different deletions in the B2 loop consistently lowered Γ_{attack} by an order of magnitude (Table 2). This suggested that the B2 loop is vital for the ability of TrCel7A to attack variable surface structures. Conversely, deletions in the B3 and B4 loops only produced negligible changes in Γ_{attack}, and we deduce that these loops are of minor importance for the ability to thread and convert different structures on the surface. It is interesting to compare these attack site densities with the maximal adsorption capacities, Γ_{max}, derived from the binding isotherms in Table 2 and Fig. 2*C*. Unlike Γ_{attack}, we found that Γ_{max} varied only moderately between the investigated enzymes, and this suggests that the studied loops are relatively unimportant for the enzymes' ability to adsorb onto Avicel. Taken together, these results show that the B2 loop is crucial for the ability to form catalytically competent complexes on different surface structures, but not for adsorption *per se*. Overall, both conventional and inverse steady-state analyses highlighted the B2 loop as a key determinant of TrCel7A's function as a CBH. Conversely, kinetic parameters of the ΔB3 and ΔB4 variants were only marginally changed compared with WT TrCel7A, and we conclude that these loops played minor roles for the distinction between CBH- and EG-like function.

Activity on other cellulosic substrates

CBHs and EGs differ with respect to their preference for different types of cellulosic substrates. Typically, EGs are most active on amorphous substrates, whereas CBHs are particularly effective degraders of crystalline cellulose (10). To assess these differences for the loop variants, we made end-point activity measurements on regenerated amorphous cellulose (RAC; predominantly amorphous cellulose) and bacterial microcrystalline cellulose (BMCC; predominantly crystalline cellulose). Results shown in Fig. 3 confirmed the typical preferences of CBH and EG WTs mentioned above. More importantly, we found that the loop variants showed intermediate preferences. Again, these results followed the picture where the three ΔB2 variants shifted distinctively toward a more EG-like behavior with a 4–5-fold increase in the activity against RAC and a loss of activity against BMCC. The analogous changes were small for the ΔB3 and ΔB4 variants, and these loops hence did not appear to be of key importance for the differences in substrate specificity.

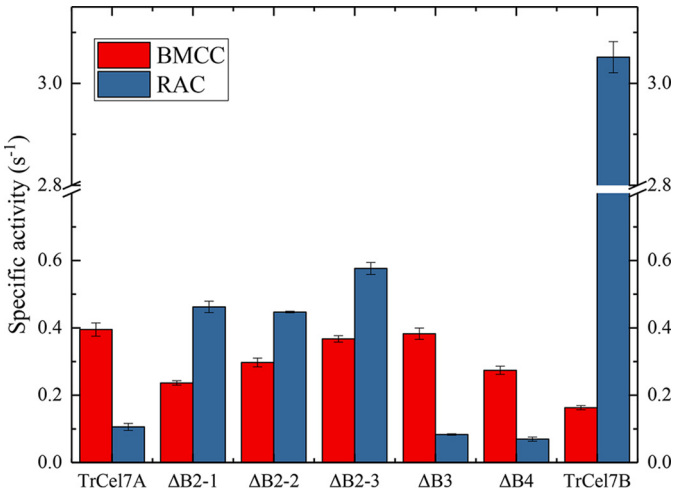

Figure 3. Specific activity (v/E_0) on cellulosic substrates with different degree of crystallinity. Conditions were as follows: 4 g/liter RAC, 50 nM enzyme or 4 g/liter BMCC, 100 nM enzyme, 25 °C, 60 min. *Error bars*, S.D.

Table 3

Relative values of endolytic activity, normalized with respect to TrCel7A

Endolytic activity was assessed on the endoglucanase-specific substrate AZCL-HE-cellulose.

Enzyme	Relative activity on AZCL-HE-cellulose
TrCel7A	1.0 ± 0.0
ΔB2-1	3.9 ± 0.3
ΔB2-2	3.8 ± 0.2
ΔB2-3	4.2 ± 0.3
ΔB3	1.2 ± 0.0
ΔB4	1.4 ± 0.1
TrCel7B	304.7 ± 12.3

Endolytic activity

The defining property of an EG is its ability to perform endolytic cleavage. To assess this, we investigated the activity against the synthetic insoluble substrate azurine-cross-linked hydroxyethylcellulose (AZCL-HE-cellulose), which is designed to elucidate endoactivity. As expected, the results in Table 3 show much higher activity on this substrate of TrCel7B compared with TrCel7A (about 300 times). For the variants, we found that the three ΔB2 variants had become more EG-like with about 4 times higher activity than TrCel7A (Table 3). For the ΔB3 and ΔB4 variants, we saw a marginal increase in the activity on AZCL-HE-cellulose. These results clearly follow the picture from kinetic data on Avicel in as much as the B2 loop appears to be particularly important for functional distinction. We note, however, that even the most active variant (ΔB2-3) was some 70 times less efficient on AZCL-HE-cellulose than TrCel7B. This clearly suggests that full endolytic activity as in TrCel7B cannot be established through the deletion of only one loop, and this probably reflects limitations in the accessibility of the substrate binding region exerted by the remaining loops and their mutual interactions. When comparing with the other kinetic data, we note that the shift toward EG-like behavior of the ΔB2 variants was less pronounced for AZCL-HE-cellulose activity (Table 3) than for kinetic parameters on real cellulose (Table 2). This may be related to the cross-linked nature of the artificial AZCL-HE substrate as well as its bulky chromogenic group, which could make this substrate particularly sensitive to reduced accessibility.

Conclusions

The kinetic parameters of TrCel7A and TrCel7B WTs in Table 2 unveil some interesting differences and similarities of these homologous enzymes. Thus, when acting on the real insoluble substrate, the EG (TrCel7B) had a maximal turnover defined in the conventional way ($^{conv}V_{max}/E_0$), which is an order of magnitude higher than the CBH (TrCel7A). The (conventional) Michaelis constant, $^{conv}K_m$, was also an order of magnitude higher for TrCel7B, and it follows that the kinetic efficiency (or specificity constant), $^{conv}V_{max}/E_0/^{conv}K_m$, was identical for the two WTs (Table 2). We used the differences in kinetic parameters for variants to elucidate functional roles of the loops. We found that the B2 loop, which covers the region around pyranose subsites −3 and −4 quite far from the catalytic residues (24, 29, 41), was particularly important for CBH-like behavior. Hence, variants with deletion of either 14, 13, or 6 residues in this loop consistently showed strong shifts toward more EG-like function. By contrast, deletions in the B3 or B4 loops were of minor importance, and these variants essentially maintained characteristic CBH kinetics as well as the ability to attack a broad range of cellulose conformations on the substrate surface. For the ΔB4 variant, the observation of moderate kinetic changes could be connected to the small size of the loop, but interestingly, the sizable deletion of 9 residues in the larger B3 loop did not have much impact on the kinetics either. These observations clearly point toward a special role of the B2 loop as a regulator of kinetic properties, and further studies of this loop appear promising for both mechanistic understanding and guidance for enzyme engineering of the industrially important GH7 family.

Experimental procedures

Design of variants

Structures of TrCel7A (PDB entry 4C4C) and TrCel7B (PDB entry 1EG1) were visualized and structurally aligned using the PyMOL Molecular Graphics System, version 2.0 (Schrödinger, LLC). The pairwise alignment was made with Clustal Omega (42) and analyzed with the ESPript 3.0 web server using default parameters (43). Details about the alignment can be found in Fig. S1.

Enzyme cloning, expression, and purification

TrCel7A and TrCel7B are cellobiohydrolase I and endoglucanase I, respectively, from *T. reesei* (*Hypocrea jecorina*). ΔB2-1, ΔB2-2, ΔB2-3, ΔB3, ΔA4, and ΔB4 are deletion variants of TrCel7A, where a specific amino acid sequence was deleted (see Fig. 1*B*). Deletions were introduced by PCR amplification of the flanking regions, which were subsequently assembled into a full-length gene using splicing by overhang extension PCR. All enzymes were expressed in *Aspergillus oryzae*, as described previously (44), and purification of enzymes from fermentation broths also followed previously described procedures (45). The purified enzyme stocks showed a single band in 15-well NuPAGE 4–12% BisTris SDS-PAGE (GE Healthcare) (Fig. S2), and the protein concentrations were determined by UV absorption at 280 nm using a theoretical extinction coefficient (46) of 86,760 M^{-1} cm^{-1} for TrCel7A, ΔA4, ΔB2-2, ΔB2–3, and ΔB4-2, 81,260 M^{-1} cm^{-1} for ΔB2-1, and 74,145 M^{-1} cm^{-1} for TrCel7B. TrCel7B was further purified by size-exclusion chromatography with a Hi Load 26/600 Superdex 75 pg column (GE Healthcare). The eluent used was 25 mM MES, pH 6, 50 mM NaCl.

Thermal stability

All enzyme characterization was performed in triplicates and with a buffer of 50 mM sodium acetate, pH 5.0, henceforth referred to as standard buffer. All chemicals were purchased at Sigma-Aldrich. Physical stability of all investigated enzymes was evaluated by DSC using MicroCal VP-Capillary DSC from Malvern Panalytical. The enzymes were buffer-changed by Vivaspin 20, 20,000 molecular weight cut-off (Sartorious, Stonehouse, Gloucestershire, UK) and suspended with standard buffer and subsequently diluted to a concentration of 0.5 mg/ml. The enzyme stability was tested with heating scans from 20 to 95 °C with a scan rate of 3.3 °C. For all enzymes, a distinct thermal transition was evident, whereas no transition was observed for the buffer scans. Data were collected and analyzed with Origin version 7 software (OriginLab, Northampton, MA), and the buffer scan was subtracted from each measurement. T_m was calculated after fitting and baseline subtraction of the obtained thermograms.

Analytical size-exclusion chromatography

To determine the structural integrity and oligomerization state of the enzymes, size-exclusion chromatography was performed. The enzymes were prepared to concentrations above 1 mg/ml and subjected to a Superdex^{TM} 75 Increase 10/300 GL column (GE Healthcare) and eluted isocratically at a flow of 0.5 ml/min with 25 mM MES and 200 mM NaCl, pH 6, buffer. Gel filtration calibration kit LMW (GE Healthcare) was used for determination of the void volume and for calibration to determine the molecular weight of the enzymes.

Activity on para-nitrophenol-β-lactoside and estimation of inhibition constant (K_i) for cellobiose

Kinetic parameters on the soluble synthetic substrate pNPL and K_i on cellobiose were estimated at 25 °C. Michaelis–Menten curves with 11 different pNPL concentrations ranging between 0.16 and 5 mM were made, in the presence or absence of cellobiose, at two concentrations: 100 and 200 μM for TrCel7A and the deletion variants, 2 and 4 mM for TrCel7B. The final enzyme concentration was 0.5 μM in all cases. The reactions were started by mixing 90 μl of pNPL at different concentrations with 60 μl of enzyme in a 96-well microtiter plate, followed by sealing and incubation at 25 °C in a ThermoMixer operating at 1,100 rpm for 30 min. The reactions were quenched by the addition of 150 μl of 1 M Na_2CO_3. 150 μl of the mixtures were then transferred to a new microtiter plate, and the concentration of the product *para*-nitrophenol (ThermoFisher, Kandel, Germany) was quantified in a spectrophotometer by measuring the absorbance at 405 nm and using a calibration curve of *para*-nitrophenol at six different concentrations (15–500 μM). Appropriate blanks were subtracted from all measurements. The experimental curves were analyzed by the software OriginPro using nonlinear regressions. To determine which inhibition mech-

anism better described the experimental data, all curves were fitted with a global fit of different inhibition models by using the small-sample corrected Akaike information criterion (31, 47, 48).

Activity on microcrystalline cellulose, conventional Michaelis–Menten (^{conv}MM)

The activity of the TrCel7A and TrCel7B WT and the six variants was tested on Avicel PH101. The substrate was washed six times in MilliQ water and three times in standard buffer. Aliquots of 230 μl of washed Avicel with loads between 0.5 and 110 g/liter were then transferred to 96-well microtiter plates (96F 26960 Thermo Scientific, Waltham, MA), and the enzymatic reaction was started by adding 20 μl of enzyme stock prepared in standard buffer to a final concentration of 50 nM. Each plate was sealed and mixed at 1,100 rpm in a ThermoMixer equipped with a ThermoTop (Eppendorf, Hamburg, Germany). The enzyme-substrate contact time was 60 min at 25 °C. The reaction was stopped by a short 3-min centrifugation at 2,000 × *g*. Volumes of 60 μl of the supernatant were retrieved and analyzed for its content of reducing sugars by using the 4-hydroxybenzoic acid hydrazide (PAHBAH) method (49). Specifically, a solution of 15 g/liter PAHBAH was dissolved in 0.177 M potassium sodium tartrate tetrahydrate and 0.5 M NaOH. 90 μl of this solution were mixed with the reaction supernatant, followed by heating at 95 °C for 10 min in a T100^{TM} PCR cycler (Bio-Rad) and cooling to 5 °C for 5 min. Finally, 100 μl were transferred into a microtiter plate, and the absorbance at 405 nm was measured by a plate reader (SpectraMax M2e, Molecular Devices, Sunnyvale, CA) using the software SoftMax Pro version 6.2, Molecular Devices. A standard curve of 1,000 to 32.15 μM of cellobiose (Fluka) dissolved in standard buffer was included in each plate.

Binding isotherms and inverse Michaelis–Menten (^{inv}MM)

To quantify enzyme adsorption on microcrystalline cellulose, a constant substrate load of Avicel was used, and the enzyme concentration varied between 0.05 and 6 μM. The enzymatic reaction was started by adding 60 μl of enzyme at different concentrations to microtiter plates containing 190 μl of Avicel so the final substrate concentration was 8 g/liter. The samples were mixed in a ThermoMixer for 1 h at 25 °C and then centrifuged at 2,000 × *g* for 3 min to separate free enzyme from substrate-bound enzyme. 60 μl of supernatant were mixed with 90 μl of standard buffer in a black microtiter plate (Greiner bio-one 655079), and the intrinsic protein fluorescence was measured in a plate reader by using excitation and emission wavelengths of 280 and 345 nm, respectively. The free enzyme concentration was quantified by comparing the fluorescence signal with a calibration curve made with enzyme dissolved in standard buffer with known concentrations ranging from 0.05 to 6 μM. In the *inverse MM* approach, the reaction condition was the same as for Langmuir isotherms. The reactions were incubated and analyzed for the reducing sugar content as described for the ^{conv}MM approach. Because increasing enzyme concentration affects the absorbance signal, enzyme blanks for each concentration were included.

Activity on RAC and BMCC

RAC was prepared from Avicel according to a protocol described previously (50). 230 μl of RAC suspensions dissolved in standard buffer were mixed with 20 μl of TrCel7A, TrCel7B, or the deletion variants in microtiter plates to a final enzyme concentration of 50 nM and a final RAC concentration of 4 g/liter. BMCC was prepared from HCl treatment of bacterial cellulose, using a protocol described previously (51). 190 μl of BMCC suspension in standard buffer were mixed with 60 μl of TrCel7A, TrCel7B, or the deletion variants in microtiter plates to a final concentration of 100 nM and a final BMCC concentration of 4 g/liter. The enzymatic reactions on RAC and BMCC were carried out at 25 °C in ThermoMixers operating at 1,100 rpm, with a contact time of 1 h. The reactions were stopped by centrifugation, and the reducing sugar content was analyzed using PAHBAH, as described previously.

Endolytic activity on AZCL-HE-cellulose

Endolytic activity of the enzymes was estimated with the chromogenic insoluble substrate AZCL-HE-cellulose (Megazyme, Bray, Ireland). A stock suspension of AZCL-HE-cellulose in standard buffer at a concentration of 5 g/liter was prepared, and aliquots of 90 μl were transferred to transparent microtiter plates. The enzyme reaction was started by adding 60 μl of enzyme stock to a total final enzyme concentration of 5 μM. The plates were incubated at 25 °C in a ThermoMixer with ThermoTop. For TrCel7A and deletion variants, the reaction time was 2 h, and for TrCel7B, it was 15 min. The reactions were stopped by adding 150 μl of NaOH 0.1 M, followed by centrifugation for 3 min at 2,000 × *g*. 100 μl of the supernatant was transferred to microtiter plates, and the adsorption at 595 nm was measured in a plate reader. Activity was expressed as adsorption difference between reaction and a substrate blank divided by the reaction time in minutes (ΔA_{595}/min).

Author contributions—C. S.-d.-C., N. R., J. K., T. H. S., and P. W. conceptualization; C. S.-d.-C. and N. R. resources; C. S.-d.-C. and N. R. data curation; C. S.-d.-C. and N. R. software; C. S.-d.-C., and N. R. formal analysis; C. S.-d.-C., N. R., and J. K. validation; C. S. d. C. and N. R. investigation; C. S. d. C., N. R., K. J., and J. K. methodology; C. S.-d.-C., N. R., and P. W. writing-original draft; C. S.-d.-C., N. R., K. B., and P. W. writing-review and editing; K. J. supervision; K. B. and P. W. funding acquisition; K. B. and P. W. project administration.

Acknowledgment—We thank Senior Research Associate Ria Jacobsson (Novozymes) for technical assistance with the cloning procedure.

References

1. Penttilä, M., Lehtovaara, P., Nevalainen, H., Bhikhabhai, R., and Knowles, J. (1986) Homology between cellulase genes of *Trichoderma reesei*: complete nucleotide sequence of the endoglucanase I gene. *Gene* **45,** 253–263 CrossRef Medline
2. Rosgaard, L., Pedersen, S., Langston, J., Akerhielm, D., Cherry, J. R., and Meyer, A. S. (2007) Evaluation of minimal *Trichoderma reesei* cellulase mixtures on differently pretreated barley straw substrates. *Biotechnol. Prog.* **23,** 1270–1276 CrossRef Medline
3. Herpoël-Gimbert, I., Margeot, A., Dolla, A., Jan, G., Mollé, D., Lignon, S., Mathis, H., Sigoillot, J.-C., Monot, F., and Asther, M. (2008) Comparative secretome analyses of two *Trichoderma reesei* RUT-C30 and CL847 hypersecretory strains. *Biotechnol. Biofuels* **1,** 18 CrossRef Medline

4. Saloheimo, M., and Pakula, T. M. (2012) The cargo and the transport system: secreted proteins and protein secretion in *Trichoderma reesei* (*Hypocrea jecorina*). *Microbiology* **158,** 46–57 CrossRef Medline
5. Praestgaard, E., Elmerdahl, J., Murphy, L., Nymand, S., McFarland, K. C., Borch, K., and Westh, P. (2011) A kinetic model for the burst phase of processive cellulases. *FEBS J.* **278,** 1547–1560 CrossRef Medline
6. Cruys-Bagger, N., Elmerdahl, J., Praestgaard, E., Tatsumi, H., Spodsberg, N., Borch, K., and Westh, P. (2012) Pre-steady state kinetics for the hydrolysis of insoluble cellulose by cellobiohydrolase Cel7A. *J. Biol. Chem.* **287,** 18451–18458 CrossRef Medline
7. Knott, B. C., Haddad Momeni, M., Crowley, M. F., Mackenzie, L. F., Götz, A. W., Sandgren, M., Withers, S. G., Ståhlberg, J., and Beckham, G. T. (2014) The mechanism of cellulose hydrolysis by a two-step, retaining cellobiohydrolase elucidated by structural and transition path sampling studies. *J. Am. Chem. Soc.* **136,** 321–329 CrossRef Medline
8. Ståhlberg, J., Divne, C., Koivula, A., Piens, K., Claeyssens, M., Teeri, T. T., and Jones, T. A. (1996) Activity studies and crystal structures of catalytically deficient mutants of cellobiohydrolase I from *Trichoderma reesei*. *J. Mol. Biol.* **264,** 337–349 CrossRef Medline
9. Kurašin, M., and Väljamäe, P. (2011) Processivity of cellobiohydrolases is limited by the substrate. *J. Biol. Chem.* **286,** 169–177 CrossRef Medline
10. Zhang, Y. H. P., and Lynd, L. R. (2004) Toward an aggregated understanding of enzymatic hydrolysis of cellulose: noncomplexed cellulase systems. *Biotechnol. Bioeng.* **88,** 797–824 CrossRef Medline
11. Bu, L., Nimlos, M. R., Shirts, M. R., Ståhlberg, J., Himmel, M. E., Crowley, M. F., and Beckham, G. T. (2012) Product binding varies dramatically between processive and nonprocessive cellulase enzymes. *J. Biol. Chem.* **287,** 24807–24813 CrossRef Medline
12. Jalak, J., Kurašin, M., Teugjas, H., and Väljamäe, P. (2012) Endo-exo synergism in cellulose hydrolysis revisited. *J. Biol. Chem.* **287,** 28802–28815 CrossRef Medline
13. Ståhlberg, J., Johansson, G., and Pettersson, G. (1993) *Trichoderma reesei* has no true exo-cellulase: all intact and truncated cellulases produce new reducing end groups on cellulose. *Biochim. Biophys. Acta* **1157,** 107–113 CrossRef Medline
14. Olsen, J. P., Kari, J., Borch, K., and Westh, P. (2017) A quenched-flow system for measuring heterogeneous enzyme kinetics with sub-second time resolution. *Enzyme Microbial Technol.* **105,** 45–50 CrossRef Medline
15. Murphy, L., Bohlin, C., Baumann, M. J., Olsen, S. N., Sørensen, T. H., Anderson, L., Borch, K., and Westh, P. (2013) Product inhibition of five *Hypocrea jecorina* cellulases. *Enzyme Microbial Technol.* **52,** 163–169 CrossRef Medline
16. Teugjas, H., and Väljamäe, P. (2013) Product inhibition of cellulases studied with 14 C-labeled cellulose substrates. *Biotechnol. Biofuels* **6,** 104 CrossRef Medline
17. Pellegrini, V. O., Lei, N., Kyasaram, M., Olsen, J. P., Badino, S. F., Windahl, M. S., Colussi, F., Cruys-Bagger, N., Borch, K., and Westh, P. (2014) Reversibility of substrate adsorption for the cellulases Cel7A, Cel6A, and Cel7B from *Hypocrea jecorina*. *Langmuir* **30,** 12602–12609 CrossRef Medline
18. Henrissat, B., Driguez, H., Viet, C., and Schülein, M. (1985) Synergism of cellulases from *Trichoderma reesei* in the degradation of cellulose. *Nat. Biotechnol.* **3,** 722–726 CrossRef
19. Kostylev, M., and Wilson, D. (2012) Synergistic interactions in cellulose hydrolysis. *Biofuels* **3,** 61–70 CrossRef
20. Väljamäe, P., Sild, V., Nutt, A., Pettersson, G., and Johansson, G. (1999) Acid hydrolysis of bacterial cellulose reveals different modes of synergistic action between cellobiohydrolase I and endoglucanase I. *Eur. J. Biochem.* **266,** 327–334 CrossRef Medline
21. Divne, C., Ståhlberg, J., Reinikainen, T., Ruohonen, L., Pettersson, G., Knowles, J. K., Teeri, T. T., and Jones, T. A. (1994) The three-dimensional crystal structure of the catalytic core of cellobiohydrolase I from *Trichoderma reesei*. *Science* **265,** 524–528 CrossRef Medline
22. Kleywegt, G. J., Zou, J.-Y., Divne, C., Davies, G. J., Sinning, I., Ståhlberg, J., Reinikainen, T., Srisodsuk, M., Teeri, T. T., and Jones, T. A. (1997) The crystal structure of the catalytic core domain of endoglucanase I from *Trichoderma reesei* at 3.6 Å resolution, and a comparison with related enzymes. *J. Mol. Biol.* **272,** 383–397 CrossRef Medline
23. Mertz, B., Gu, X., and Reilly, P. J. (2009) Analysis of functional divergence within two structurally related glycoside hydrolase families. *Biopolymers* **91,** 478–495 CrossRef Medline
24. Momeni, M. H., Payne, C. M., Hansson, H., Mikkelsen, N. E., Svedberg, J., Engström, Å., Sandgren, M., Beckham, G. T., and Ståhlberg, J. (2013) Structural, biochemical, and computational characterization of the glycoside hydrolase family 7 cellobiohydrolase of the tree-killing fungus *Heterobasidion irregulare*. *J. Biol. Chem.* **288,** 5861–5872 CrossRef Medline
25. Hobdey, S. E., Knott, B. C., Haddad Momeni, M., Taylor, L. E., 2nd, Borisova, A. S., Podkaminer, K. K., VanderWall, T. A., Himmel, M. E., Decker, S. R., Beckham, G. T., and Ståhlberg, J. (2016) Biochemical and structural characterization of two *Dictyostelium* cellobiohydrolases from the Amoebozoa kingdom reveal a high conservation between distant phylogenetic trees of life. *Appl. Environ. Microbiol.* **82,** 3395–3409 CrossRef Medline
26. Meinke, A., Damude, H. G., Tomme, P., Kwan, E., Kilburn, D. G., Miller, R. C., Jr., Warren, R. A. J., and Gilkes, N. R. (1995) Enhancement of the endo-β-1,4-glucanase activity of an exocellobiohydrolase by deletion of a surface loop. *J. Biol. Chem.* **270,** 4383–4386 CrossRef Medline
27. von Ossowski, I., Ståhlberg, J., Koivula, A., Piens, K., Becker, D., Boer, H., Harle, R., Harris, M., Divne, C., Mahdi, S., Zhao, Y., Driguez, H., Claeyssens, M., Sinnott, M. L., and Teeri, T. T. (2003) Engineering the exo-loop of *Trichoderma reesei* cellobiohydrolase, Cel7A: a comparison with *Phanerochaete chrysosporium* Cel7D. *J. Mol. Biol.* **333,** 817–829 CrossRef Medline
28. Silveira, R. L., and Skaf, M. S. (2018) Concerted motions and large-scale structural fluctuations of Trichoderma reesei Cel7A cellobiohydrolase. *Phys. Chem. Chem. Phys.* **20,** 7498–7507 CrossRef Medline
29. Taylor, C. B., Payne, C. M., Himmel, M. E., Crowley, M. F., McCabe, C., and Beckham, G. T. (2013) Binding site dynamics and aromatic–carbohydrate interactions in processive and non-processive family 7 glycoside hydrolases. *J. Phys. Chem. B* **117,** 4924–4933 CrossRef Medline
30. Bu, L., Crowley, M. F., Himmel, M. E., and Beckham, G. T. (2013) Computational investigation of pH dependence on loop flexibility and catalytic function in glycoside hydrolases. *J. Biol. Chem.* **288,** 12175–12186 CrossRef Medline
31. Olsen, J. P., Alasepp, K., Kari, J., Cruys-Bagger, N., Borch, K., and Westh, P. (2016) Mechanism of product inhibition for cellobiohydrolase Cel7A during hydrolysis of insoluble cellulose. *Biotechnol. Bioeng.* **113,** 1178–1186 CrossRef Medline
32. Alasepp, K., Borch, K., Cruys-Bagger, N., Badino, S., Jensen, K., Sørensen, T. H., Windahl, M. S., and Westh, P. (2014) *In situ* stability of substrate-associated cellulases studied by DSC. *Langmuir* **30,** 7134–7142 CrossRef Medline
33. Jalak, J., and Väljamäe, P. (2010) Mechanism of initial rapid rate retardation in cellobiohydrolase catalyzed cellulose hydrolysis. *Biotechnol. Bioeng.* **106,** 871–883 CrossRef Medline
34. Kari, J., Olsen, J., Borch, K., Cruys-Bagger, N., Jensen, K., and Westh, P. (2014) Kinetics of cellobiohydrolase (Cel7A) variants with lowered substrate affinity. *J. Biol. Chem.* **289,** 32459–32468 CrossRef Medline
35. Bezerra, R. M., and Dias, A. A. (2004) Discrimination among eight modified Michaelis-Menten kinetics models of cellulose hydrolysis with a large range of substrate/enzyme ratios. *Appl. Biochem. Biotechnol.* **112,** 173–184 CrossRef Medline
36. Cruys-Bagger, N., Elmerdahl, J., Praestgaard, E., Borch, K., and Westh, P. (2013) A steady-state theory for processive cellulases. *FEBS J.* **280,** 3952–3961 CrossRef Medline
37. Kari, J., Andersen, M., Borch, K., and Westh, P. (2017) An inverse Michaelis–Menten approach for interfacial enzyme kinetics. *ACS Catalysis* **7,** 4904–4914 CrossRef
38. Andersen, M., Kari, J., Borch, K., and Westh, P. (2018) Michaelis–Menten equation for degradation of insoluble substrate. *Math. Biosci.* **296,** 93–97 CrossRef Medline
39. Bailey, C. J. (1989) Enzyme kinetics of cellulose hydrolysis. *Biochem. J.* **262,** 1001 Medline
40. Badino, S. F., Kari, J., Christensen, S. J., Borch, K., and Westh, P. (2017) Direct kinetic comparison of the two cellobiohydrolases Cel6A and Cel7A from *Hypocrea jecorina*. *Biochim. Biophys. Acta Proteins Proteom.* **1865,** 1739–1745 CrossRef Medline

41. Divne, C., Ståhlberg, J., Teeri, T. T., and Jones, T. A. (1998) High-resolution crystal structures reveal how a cellulose chain is bound in the 50 Å long tunnel of cellobiohydrolase I from *Trichoderma reesei*. *J. Mol. Biol.* **275,** 309–325 CrossRef Medline
42. Sievers, F., Wilm, A., Dineen, D., Gibson, T. J., Karplus, K., Li, W., Lopez, R., McWilliam, H., Remmert, M., Söding, J., Thompson, J. D., and Higgins, D. G. (2011) Fast, scalable generation of high-quality protein multiple sequence alignments using Clustal Omega. *Mol. Syst. Biol.* **7,** 539 Medline
43. Robert, X., and Gouet, P. (2014) Deciphering key features in protein structures with the new ENDscript server. *Nucleic Acids Res.* **42,** W320–W324 CrossRef Medline
44. Borch, K., Jensen, K., Krogh, K., McBrayer, B., Westh, P., Kari, J., Olsen, J., Sørensen, T. H., Windahl, M. S., and Xu, H. (December 9, 2014) Cellobiohydrolase variants and polynucleotides encoding same. International Patent WO2014138672
45. Sørensen, T. H., Cruys-Bagger, N., Windahl, M. S., Badino, S. F., Borch, K., and Westh, P. (2015) Temperature effects on kinetic parameters and substrate affinity of Cel7A cellobiohydrolases. *J. Biol. Chem.* **290,** 22193–22202 CrossRef Medline
46. Pace, C. N., Vajdos, F., Fee, L., Grimsley, G., and Gray, T. (1995) How to measure and predict the molar absorption coefficient of a protein. *Protein Sci.* **4,** 2411–2423 CrossRef Medline
47. Akpa, O. M., and Unuabonah, E. I. (2011) Small-sample corrected Akaike information criterion: an appropriate statistical tool for ranking of adsorption isotherm models. *Desalination* **272,** 20–26 CrossRef
48. Kletting, P., Kull, T., Reske, S. N., and Glatting, G. (2009) Comparing time activity curves using the Akaike information criterion. *Phys. Med. Biol.* **54,** N501-7 CrossRef Medline
49. Lever, M. (1973) Colorimetric and fluorometric carbohydrate determination with *p*-hydroxybenzoic acid hydrazide. *Biochem. Med.* **7,** 274–281 CrossRef Medline
50. Zhang, Y.-H. P., Cui, J., Lynd, L. R., and Kuang, L. R. (2006) A transition from cellulose swelling to cellulose dissolution by *o*-phosphoric acid: evidence from enzymatic hydrolysis and supramolecular structure. *Biomacromolecules* **7,** 644–648 CrossRef Medline
51. Velleste, R., Teugjas, H., and Väljamäe, P. (2010) Reducing end-specific fluorescence labeled celluloses for cellulase mode of action. *Cellulose* **17,** 125–138 CrossRef

Systematic deletions in the cellobiohydrolase (CBH) Cel7A from the fungus *Trichoderma reesei* reveal flexible loops critical for CBH activity

Corinna Schiano-di-Cola, Nanna Røjel, Kenneth Jensen, Jeppe Kari, Trine Holst Sørensen, Kim Borch and Peter Westh

J. Biol. Chem. 2019, 294:1807-1815.
doi: 10.1074/jbc.RA118.006699 originally published online December 11, 2018